Reduced CD36-dependent tissue sequestration of *Plasmodium*-infected erythrocytes is detrimental to malaria parasite growth in vivo

Jannik Fonager,[1] Erica M. Pasini,[4] Joanna A.M. Braks,[1] Onny Klop,[1] Jai Ramesar,[1] Edmond J. Remarque,[4] Irene O.C.M. Vroegrijk,[2] Sjoerd G. van Duinen,[3] Alan W. Thomas,[4] Shahid M. Khan,[1] Matthias Mann,[5] Clemens H.M. Kocken,[4] Chris J. Janse,[1] and Blandine M.D. Franke-Fayard[1]

[1]Leiden Malaria Research Group, Department of Parasitology, [2]Department of Endocrinology, [3]Department of Pathology, Leiden University Medical Center, 2333 ZA Leiden, Netherlands
[4]Department of Parasitology, Biomedical Primate Research Centre, 2280 GH Rijswijk, Netherlands
[5]Department of Proteomics and Signal Transduction, Max-Planck Institute, D-82152 Martinsried, Germany

Adherence of parasite-infected red blood cells (irbc) to the vascular endothelium of organs plays a key role in the pathogenesis of *Plasmodium falciparum* malaria. The prevailing hypothesis of why irbc adhere and sequester in tissues is that this acts as a mechanism of avoiding spleen-mediated clearance. Irbc of the rodent parasite *Plasmodium berghei ANKA* sequester in a fashion analogous to *P. falciparum* by adhering to the host receptor CD36. To experimentally determine the significance of sequestration for parasite growth, we generated a mutant *P. berghei ANKA* parasite with a reduced CD36-mediated adherence. Although the cognate parasite ligand binding to CD36 is unknown, we show that non-sequestering parasites have reduced growth and we provide evidence that in addition to avoiding spleen removal, other factors related to CD36-mediated sequestration are beneficial for parasite growth. These results reveal for the first time the importance of sequestration to a malaria infection, with implications for the development of strategies aimed at reducing pathology by inhibiting tissue sequestration.

CORRESPONDENCE
Blandine M.D. Franke-Fayard:
bfranke@lumc.nl

Abbreviations used: GR assay, growth rate assay; HL, hypotonic lysis; HMM, hidden Markov model; hpi, hours post invasion; irbc, infected rbc; PFG, pulse-field gel; rbc, red blood cells; SMAC, schizont membrane-associated cytoadherence protein; SS, surface shaving.

In humans the spleen plays a crucial role in defense against infections with viruses, bacteria, fungi, and parasites. Important functions of the spleen include removal of old and abnormal blood cells, removal of circulating pathogens, and facilitating development of immune responses against these pathogens (Mebius and Kraal, 2005). Malaria is an infectious disease caused by *Plasmodium* parasites and it is intimately associated with forms of the parasite that invade and multiply within red blood cells (rbc). It has been shown that the spleen plays an active role in the retention and removal of malaria-infected rbc (irbc) from the blood circulation (Engwerda et al., 2005; Buffet et al., 2011) and has a central role in the development of immune responses directed against the parasites (Langhorne et al., 2004; Engwerda et al., 2005).

Recognition of irbc by the spleen may result from alterations in erythrocyte membrane rigidity induced by changes in the composition and/or distribution of erythrocyte proteins/molecules or through the exposure of *Plasmodium*-specific proteins on or at the irbc surface membrane (Maier et al., 2009; Buffet et al., 2011). The human malaria parasite *Plasmodium falciparum* actively remodels the host erythrocyte through exporting parasite proteins into the host cytoplasm and to the irbc surface (Maier et al., 2009; Goldberg and Cowman, 2010). This remodeling can lead to alterations in irbc deformability and changes in surface membrane protein composition (Dondorp et al., 2000; Maier et al., 2009). One of the best characterized

J. Fonager and E.M. Pasini contributed equally to this paper.

The Rockefeller University Press $30.00
J. Exp. Med. Vol. 209 No. 1 93-107
www.jem.org/cgi/doi/10.1084/jem.20110762

P. falciparum proteins exposed on the irbc surface is PfEMP1, a variant antigen encoded by the family of so-called *var* genes (Scherf et al., 2008; Maier et al., 2009). This protein mediates adhesion to several receptors present on endothelial cells of the microvasculature, such as CD36 and ICAM1 (Sherman et al., 2003; Chakravorty and Craig, 2005; Rowe et al., 2009) and to chondroitin sulfate (CSA) that is present on the surface of syncytiotrophoblasts of the placenta (Fried and Duffy, 1996; Srivastava et al., 2010). PfEMP1-mediated adherence results in tissue sequestration of irbc, removing them from the peripheral blood circulation. The prevailing hypothesis for why irbc sequestration occurs is that it prevents spleen-mediated clearance of irbc and thus benefits the parasite survival and maintenance of an infection (Sherman et al., 2003; Buffet et al., 2011). Sequestration of irbc in the microvasculature of organs such as the lungs, brain, and placenta is thought to directly contribute to severe pathologies associated with *P. falciparum* infections, such as cerebral malaria and pregnancy-associated malaria (Rogerson et al., 2007; Mishra and Newton, 2009). It has been shown that sequestration of irbc can lead to vascular obstruction, metabolic disturbances such as acidosis and local endothelial cell activation, and release of proinflammatory cytokines (Miller et al., 2002; Schofield and Grau, 2005; Mishra and Newton, 2009). Because of the central role of irbc sequestration in malaria pathogenesis, strategies are being pursued to develop anti-adhesion adjunctive therapies for reducing sequestration and thereby reducing severe disease and mortality (Rowe et al., 2009; Avril et al., 2010; John et al., 2010). Such anti-adhesion therapies may reduce pathology directly by reducing parasite loads in critical tissues or may also result in decreased rate of parasite expansion (e.g., growth rate) as a result of the removal of nonsequestering irbc by the spleen. However, how sequestration affects parasite growth and avoidance of spleen-mediated clearance has not been experimentally validated and remains largely unknown.

In this study, we have used a rodent model of malaria, *Plasmodium berghei ANKA*, to experimentally assess in vivo the importance of tissue sequestration on parasite growth rate and spleen-mediated removal of irbc. *P. berghei ANKA* sequesters in a fashion analogous to *P. falciparum* in that irbc containing the maturing forms (schizonts) are not present in the peripheral blood but are sequestered in organs such as the lungs and adipose tissue (Franke-Fayard et al., 2005, 2010; Spaccapelo et al., 2010). Moreover, *P. berghei ANKA* irbc adhere to the class II scavenger receptor CD36 (Franke-Fayard et al., 2005), which is also one of the major human receptors to which *P. falciparum* irbc adhere. In contrast to *P. falciparum*, where PfEMP1 has been identified as the critical parasite ligand that binds to CD36, a *P. berghei ANKA* protein responsible for CD36-mediated adherence remains to be identified because the *P. berghei ANKA* genome does not contain any direct orthologues of the PfEMP1-encoding *var* genes (Hall et al., 2005). This is despite human and mouse CD36 showing high sequence and structural similarity (Silverstein and Febbraio, 2009). In our study, we have used a proteomic analysis of *P. berghei ANKA* irbc membranes to identify parasite proteins associated with the erythrocyte membrane. We identified a small protein, schizont membrane-associated cytoadherence protein (SMAC), that is exported into the cytoplasm of the host erythrocyte. Mutants lacking expression of SMAC show a strongly reduced CD36-mediated irbc sequestration. Analysis of the growth rate of this parasite in splenectomized and nonsplenectomized WT and CD36$^{-/-}$ mice in combination with real time in vivo analysis of tissue distribution of irbc demonstrate that CD36-mediated sequestration benefits parasite growth. This study is the first experimental validation of the beneficial role of sequestration for the *Plasmodium* parasite, and we discuss the possible consequences of these observations for intervention strategies directed against parasite sequestration.

RESULTS

Identification of proteins putatively involved in *P. berghei ANKA*–irbc cytoadherence

In contrast to *P. falciparum*, where PfEMP1 has been identified as the major parasite ligand that binds to CD36, the *P. berghei ANKA* protein responsible for CD36-mediated adherence is unknown, and by sequence homology the *P. berghei ANKA* genome does not contain any direct orthologs of the PfEMP1-encoding *var* genes (Hall et al., 2005; GeneDB, www.genedb.org). Furthermore, using hidden Markov model (HMM) building we were unable to unequivocally identify *P. berghei ANKA* proteins with the known CD36-binding CIDR domain of *P. falciparum* PfEMP1 and only a few proteins were identified with weak sequence identity to the PfEMP1 CIDR domains (Table S1), suggesting that no genes encoding PfEMP1-like domains exist in the *P. berghei* genome. Therefore, we choose to design a proteomic approach, informed by annotation, to identify putative proteins involved in cytoadherence. Two different methods were used to collect membrane fractions of Nyodenz-purified irbc (2–3 × 10^8), highly enriched with maturing schizonts, i.e. the hypotonic lysis (HL) method (Pasini et al., 2006) and the surface shaving (SS) method. These schizonts were collected at 23 h after merozoite invasion from synchronized in vitro cultures of *P. berghei ANKA* blood stages. For the HL method, irbc were lysed and membrane fractions collected by differential centrifugation. This method is expected to yield not only irbc surface membranes but also other membrane components present in the irbc cytosol (Pasini et al., 2006). The proteins of the membrane-enriched fractions were separated on a one-dimensional SDS-PAGE, and protein-containing bands were isolated and digested in gel with trypsin. For the SS method, intact irbc were incubated with trypsin and surface-released proteins were collected by differential centrifugation. This method is expected to mainly yield proteins that are exposed on the surface membrane of irbc. Samples of both methods were analyzed by capillary liquid chromatography coupled online with tandem mass-spectrometry (LC-MS/MS). Searching the MS/MS spectra against a database of tryptic peptides predicted from all *P. berghei ANKA* proteins resulted in identification of 289 and 265 proteins in the

HL and SS proteomes, respectively (Table S2). Because we used irbc containing maturing schizonts, it is expected that a fraction of schizonts will rupture during sample preparation, resulting in the release of free merozoites. As a consequence, the SS samples will not only contain proteins that are exposed on the irbc surface membrane but also on merozoite surface membranes. For further analysis, we therefore first subtracted from both the HL and SS proteome all merozoite-specific proteins that we identified in a proteome analysis of purified *P. berghei ANKA* merozoites (Table S2), resulting in a total of 244 and 41 proteins in the HL and SS proteomes, respectively (Table S2). The SS proteome is significantly enriched for proteins with a signal sequence, the *Plasmodium* export element (PEXEL), and for proteins predicted to be exported into the erythrocyte (Sargeant et al., 2006; Table S2 and Table S3). From the SS and HL proteome, we selected 30 proteins for further analysis of a possible role in irbc sequestration. The protein selection was based on at least one of the following criteria (Table S4): presence of export- or membrane-related features such as a signal sequence, transmembrane domain, GPI-anchor, or PEXEL motif; predicted role of the identified protein or protein domain in adhesion and/or protein export (based on the functional annotation available from PlasmoDB, www.plasmodb.org; 2006, release 5.2); proteins encoded by subtelomerically located gene families with proposed antigenic properties. See Table S1 for results of HMM searches for *P. berghei ANKA* proteins containing a PEXEL motif. We excluded exported genes belonging to the *bir* and *Pb-fam-3* (*pyst-b*) multigene families (Table S2; GeneDB, www.genedb.org) because analysis of several of these proteins did not reveal evidence for a surface membrane location or involvement in sequestration (Franke-Fayard et al., 2010; unpublished data), nor were they present in the SS proteome (Table S2).

Identification of a protein, SMAC, involved in sequestration of *P. berghei ANKA* schizonts

A genetic and phenotypic screen was used to identify the role of the 30 selected proteins in irbc sequestration. Using standard methods of reverse genetics in *P. berghei ANKA* (Janse et al., 2006), we targeted all 30 genes for permanent deletion using DNA-targeting constructs (Table S4 and Fig. S1). All gene deletion mutants were generated in a reference reporter *P. berghei ANKA* line, WT-GFP-Luc$_{schiz}$, expressing the fusion protein GFP-Luciferase under the control of the schizont-specific *ama1* promoter (Spaccapelo et al., 2010). This reporter line enables the quantification of the number of schizont irbc in peripheral blood (tail blood) by FACS analysis and the quantification of tissue distribution of irbc using real time in vivo imaging (Franke-Fayard et al., 2005, 2006). We were unable to delete 11 of the 30 genes (two to four independent transfection experiments per gene; Table S4), indicating an essential role of these proteins during asexual blood stage development. For the remaining 19 genes, we were able to select gene-deletion mutant parasites (Table S4), and the correct disruption of these genes was confirmed by Southern analysis of separated chromosomes and/or diagnostic PCR. Details of the DNA constructs and the genotype analysis of all mutants have been submitted to the RMgm database of genetically modified rodent malaria parasites (www.pberghei.eu). The 19 mutants were screened in two phenotype assays: (1) in vivo growth rate of blood stages after cloning of single parasite, and (2) determination of schizonts in the peripheral blood by FACS analysis and Giemsa-stained slide analysis. 18 mutants did not show an increase in schizonts numbers in the peripheral circulation compared with WT and in 13 of these 18 mutants there was no reduction in growth rate (Table S4). These results indicate that 18 of the 30 genes are dispensable for survival of the blood stages and do not play an essential role in CD36-mediated irbc adherence. One mutant, however, showed significantly higher numbers of schizonts in the peripheral blood circulation of infected mice compared with mice infected with WT *P. berghei ANKA*, as was demonstrated by quantifying schizonts in tail blood both by FACS and Giemsa-stained slide analysis (Table S4 and subsequent data). This mutant lacks expression of the gene PBANKA_010060 which we have named SMAC.

SMAC is a small parasite protein exported into the cytoplasm of the rbc

The *smac* gene is located on chromosome 1, encodes a predicted 19-kD protein, and is annotated as a conserved rodent malaria protein with unknown function (GeneDB). It contains a signal sequence, a PEXEL motif (RFLVE), and a transmembrane domain (Fig. 1 A). SMAC shares features with *Plasmodium*-exported proteins of unknown function in other *Plasmodium* species (i.e., PF14_0760 and others), but (syntenic) orthologs are only found in the mouse malaria species.

Northern blot analysis of transcription in synchronized blood stages shows the presence of transcripts with a size of ~1.3 kb in developing trophozoites and schizonts with highest transcript levels in developing schizonts (Fig. 1 A). We generated two transgenic *P. berghei ANKA* lines to analyze SMAC expression and cellular localization (Fig. 1, B and C; and Fig. S1, B and C). One transgenic line, *smac*$_{5'UTR}$-mCherry, expresses mCherry under control of 1 kb of the *smac* promoter region and the other, *smac*::mCherry, expresses a (C-terminal) mCherry-tagged form of SMAC. Analyses of blood stages of *smac*$_{5'UTR}$-mCherry confirmed the pattern of expression in trophozoites and schizonts. In this mutant, the mCherry fluorescence is restricted to the cytoplasm of the different blood parasites (Fig. 1 B). In contrast, analysis of the blood stages of the *smac*::mCherry parasites showed strong mCherry fluorescence in the cytoplasm of the host erythrocyte (Fig. 1 C), demonstrating export of SMAC into the host erythrocyte. In synchronized blood stages, weak SMAC::mCherry was detected in the cytoplasm of developing trophozoites (5–12 h). Fluorescence increased in maturing trophozoites and schizonts with a patchy fluorescent signal in the cytoplasm of rbc infected with immature and mature schizonts (Fig. 1 C). We did not observe SMAC::mCherry at or close to the irbc surface membrane. The localization of SMAC::mCherry is clearly different from the irbc surface

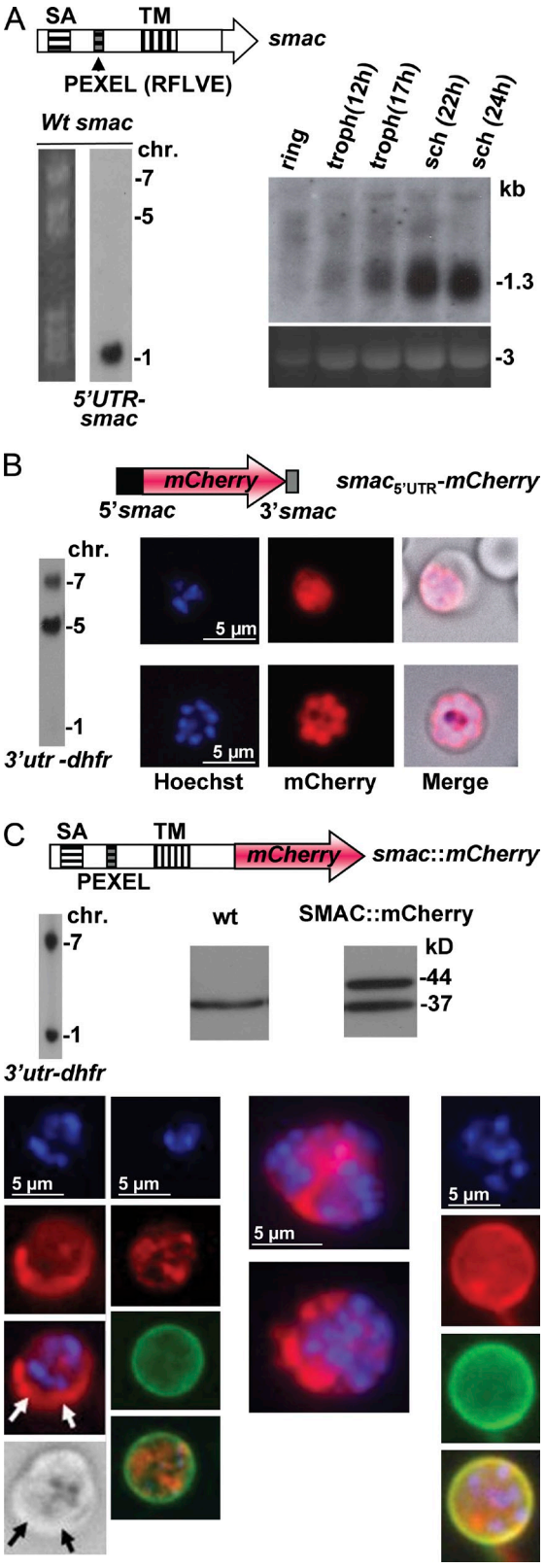

Figure 1. SMAC expression in trophozoites and schizonts and its localization in the cytoplasm of the infected erythrocyte. (A) Location of the signal anchor (SA), PEXEL motif, and transmembrane domain (TM) in SMAC (top), location of *smac* on PFG-separated chromosomes (chr.), and transcription in blood stages (troph, trophozoites; sch, schizonts). Blots were hybridized to the 5′UTR *smac* probe. (B) mCherry expression in blood stages of line $smac_{5'UTR}$-mCherry, which contains mCherry with the regulatory sequences of *smac* integrated into the *c/d-ssu-rrna* locus (chromosome 5). Fluorescence is restricted to the cytoplasm of (maturing) trophozoites (top row) and schizonts (bottom row). (C) mCherry expression in blood stages of line SMAC::mCherry, which contains an mCherry-tagged version of *smac* on chromosome 1. Western analysis using mCherry antibodies detects the 44-kD SMAC::mCherry protein (SMAC, 15 kD; mCherry, 29 kD) in schizonts. These antibodies also hybridize aspecifically to a 37-kD protein which is used as a loading control for WT parasites. (Left two columns) mCherry fluorescence (red) is detected in the cytoplasm of schizont-irbc. mCherry fluorescence is mainly detected in the cytoplasm (arrows) and not in/on the irbc surface membrane, which is stained with anti-mouse TER119 (green). (Middle column) Schizonts showing SMAC::mCherry localization in the irbc cytoplasm. (Right column) An example of irbc surface localization of a *P. berghei ANKA* protein in schizonts. This protein, PBANKA_083680, is C-terminally tagged with mCherry (red) and the irbc surface membrane colors yellow when mCherry fluorescence is merged with anti-mouse TER119 fluorescence (green).

membrane localization of a mCherry-tagged member of the *pb-fam-1* (*pyst-a*) gene family, PBANKA_083680 (Fig. 1 C; Franke-Fayard et al., 2010). Also, the staining of live SMAC::mCherry and WT irbc with anti-mCherry or anti-SMAC antibodies did not provide evidence for exposure of SMAC on the surface of irbc (unpublished data). These antibodies, generated against the peptide CTHGQYKYHRNNVYT-amide (corresponding to a region located N-terminal of the transmembrane domain and downstream of the PEXEL motif) recognized the SMAC protein in both Western and immunoprecipitation analyses. These results suggest that the lack of sequestration of Δ*smac* schizonts is not a result of SMAC's direct involvement in binding to host endothelial receptors but most likely affects the surface exposure of additional proteins that are responsible for irbc sequestration. Although SMAC is unlikely to be the *P. berghei* ligand binding to endothelial CD36 (described in more detail in the following sections) parasites lacking SMAC show a strong reduction in irbc sequestration. They thereby serve to illustrate the role of CD36-mediated irbc sequestration.

Blood stages of Δ*smac* parasites have a normal cell cycle but are affected in CD36-mediated schizont sequestration

We generated three independent gene deletion mutants, Δ*smac1-3*, lacking expression of SMAC, two using a standard positive selectable marker, and Δ*smac3* was generated using the positive-negative selection cassette *hdhfr-fcu* (Figs. S1 and S2). For the three mutants, correct gene deletion was confirmed by diagnostic PCR, Southern analysis, and loss of SMAC expression by Western analysis (Fig. 2 A and Fig. S2). The multiplication rate of blood stage Δ*smac* parasites, which is defined as the fold increase in parasite numbers in mice during the first 8–11 d after infection with a single parasite, was reduced compared with the growth rate of WT parasites (Table S4). Δ*smac* parasites showed a daily multiplication rate of 8.9 compared with a 10× multiplication rate in WT parasites.

Standard analysis of cell cycle progression by flow cytometry, after in vitro synchronized Hoechst-stained blood-stage parasites, revealed that Δ*smac* parasites have a cell cycle similar to WT with respect to the length of the G1 and S/M phase and the number of daughter cells produced during the S/M phase of the cell cycle. As in WT, the onset of the S phase was at 19 h, the first free merozoites were observed at 23 h (Fig. 2 B) and schizonts produced a similar number of daughter merozoites (Fig. 2 C). In addition, Δ*smac* parasites produced similar numbers of gametocytes compared with WT (Fig. 2 C).

In synchronized infections of WT *P. berghei ANKA* parasites, mature trophozoites rapidly and reproducibly disappear from the blood circulation at 16–18 h and >90% of the parasites that have undergone nuclear division are absent from the peripheral blood, resulting in a clear drop in parasitemia between 18 and 22 h (Franke-Fayard et al., 2010). At ∼22 h after inoculation, the first newly merozoite-invaded rbc reappear in the blood circulation. FACS analysis of the presence of schizonts in mice with synchronized Δ*smac* infections revealed that at 18 and 22 h, significantly ($P < 0.005$) more schizonts are present in the peripheral tail blood of Δ*smac*-infected mice compared with WT infected (Fig. 3, A and B). At 22 h, 26–33% of the Δ*smac* parasites are circulating schizonts, including fully mature schizonts, whereas this percentage is <8% in tail blood of WT-infected mice, which are mainly mature trophozoites with a diploid DNA content, indicating that these forms just entered schizogony (Fig. 3 A). The significantly higher numbers of circulating Δ*smac* schizonts was confirmed by counting parasites in Giemsa-stained blood films (Fig. S3 A) and measuring luciferase activity of schizonts in tail blood of mice with synchronized Δ*smac* and WT infections (Fig. 3 A). We next analyzed schizont sequestration by determining the tissue distribution of schizonts using real-time in vivo imaging in live mice (Franke-Fayard et al., 2005). This method visualizes parasite distribution in whole bodies of mice and in extracted organs by measuring luciferase activity of schizonts that express luciferase under the control of the schizont-specific *ama-1* promoter. Mice with synchronized infections of WT-GFP-Luc$_{schiz}$ and Δ*smac* parasites show clear differences in their tissue distribution of schizonts. As we have previously shown (Franke-Fayard et al., 2005), WT schizonts (18–22 h) accumulate mainly in the lungs, adipose tissue, and spleen, as demonstrated by strong luciferase

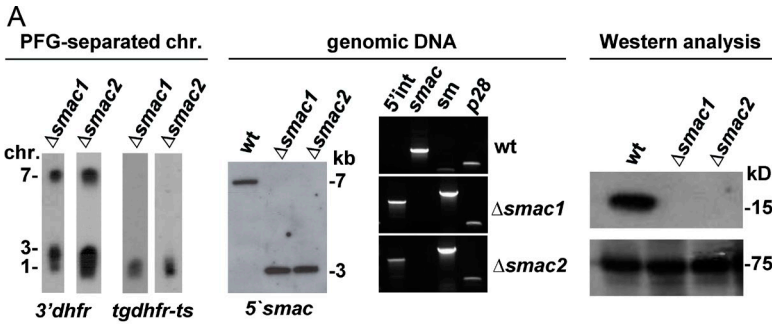

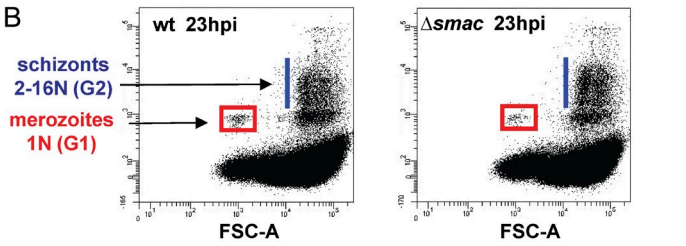

parasite	start of schizogony (length of G1 phase)		merozoite release (end of S/M phase)	
	Hours p.i.	schizonts (G2), % mean (s.d.)	Hours p.i.	merozoites (G1), %, mean (s.d.)
wt	19	13 (1)	23	13 (1)
Δ*smac*	19	22 (1)	23	9 (2)

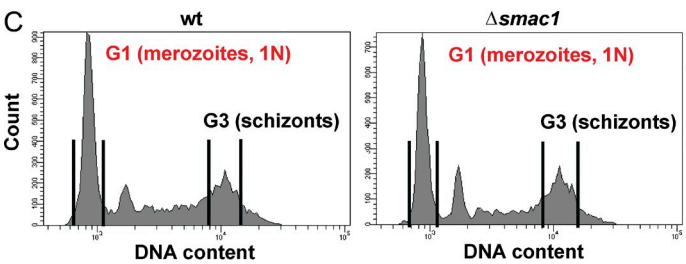

parasite	wt-1	Δ*smac1*	wt-2	Δ*smac2*
Merozoites per schizont mean no. (s.d)	13,4 (0.08)	13,2 (0.08)	12,1 (0.01	12,0 (0.03)
Gametocyte production mean (s.d.)	20.3 (4.0)	19,3 (3.1)	19,5 (2.5)	19,8 (1,9)

Figure 2. Blood stage parasites lacking expression of SMAC (Δ*smac*) show similar cell cycle characteristics to WT parasites. (A) Genotype analyses of Δ*smac* parasites. (Left) Southern analysis of PFG-separated chromosome (chr.) and *Hin*dIII-digested genomic DNA with probes recognizing the DNA-construct or the *smac*-locus show correct disruption of *smac* (see Fig. S1 D for details). (Middle) PCR confirmation of *smac*-locus disruption (5′int, 5′ region integration event; *smac*, WT *smac*; sm, selectable marker; *p28*, control PCR for the *p28* gene [PBANKA_051490]; see Fig S1 D and Table S5). (Right) Western analysis using anti-SMAC antibodies (top) confirming absence of SMAC. Hsp70 antibodies (bottom), loading control. (B) Cell cycle characteristics (length of G1 and end of the S/M phase) analyzed by FACS analysis of Hoechst-stained blood stages obtained from synchronized in vitro cultures at different hpi of erythrocytes from two independent experiments. The top shows typical dot plots of fluorescence intensity and size of cells (forward scatter) at 23 hpi. In cultures of WT and Δ*smac*, free merozoites (gate G1) are observed at 23 hpi and schizogony (gate G2: parasites with >2N DNA content) starts at 19 hpi. (C) Number of merozoites per schizont determined in cultured parasites by FACS analysis of Hoechst-stained parasites (top) from two independent experiments. Gate G1 contains the haploid free merozoites and gate G3 contains fully mature schizonts. The mean number of merozoite per schizonts (bottom) is similar in WT and Δ*smac*. Also, the gametocyte production is not different from WT parasites.

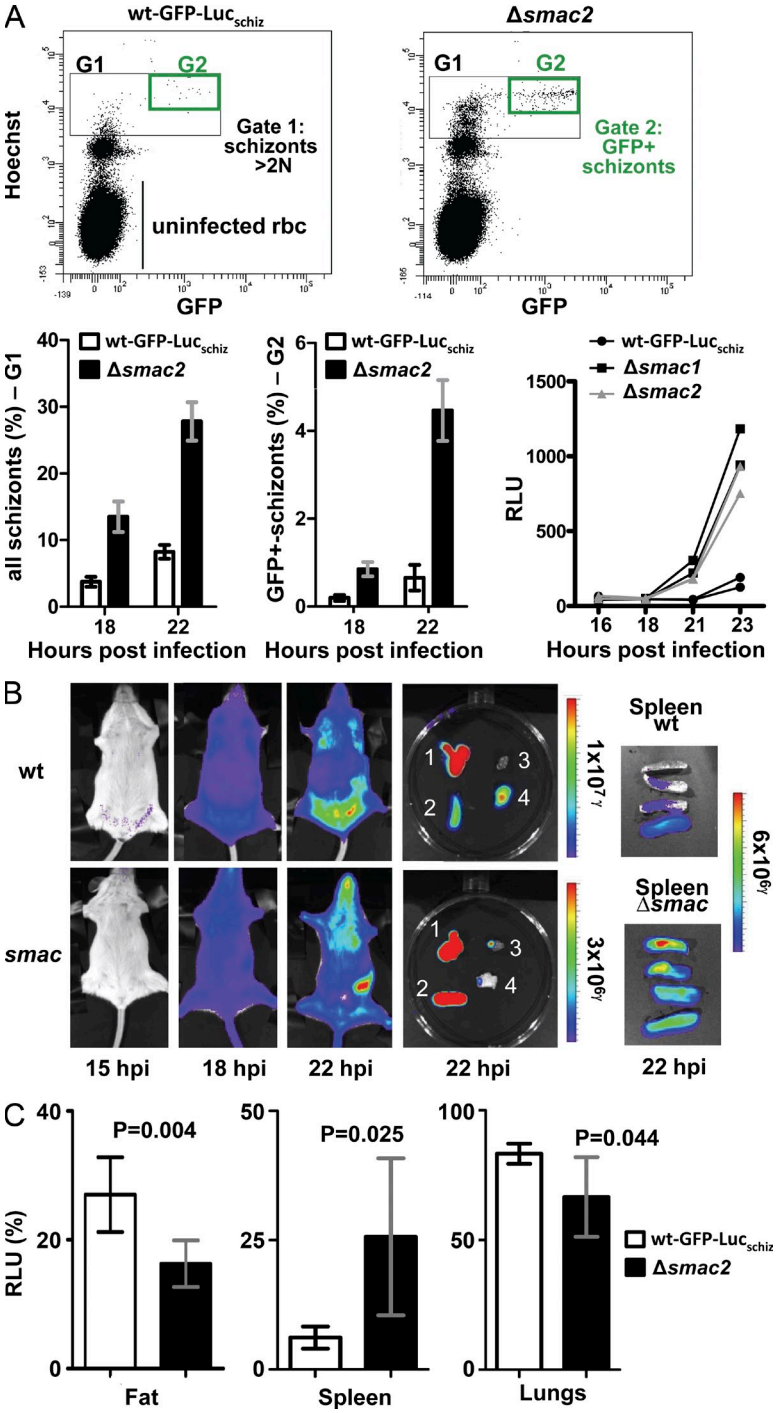

Figure 3. SMAC is involved in CD36-mediated sequestration of schizonts. (A) Analysis of the presence of schizonts in the peripheral blood circulation in mice ($n = 4$) with synchronized infections. Tail blood infected with parasites expressing GFP-Luciferase (under the *ama-1* promoter) is stained with Hoechst and analyzed for Hoechst and GFP fluorescence (top). In Δ*smac*-infected mice both the total number of schizonts (Gate G1: parasites with >2N DNA content) and mature schizonts (Gate G2: parasites expressing GFP) is significantly higher ($P < 0.004$) than in WT infected mice (bottom). Measurements of luciferase activity (RLU, relative light units) demonstrate increased numbers of luciferase-expressing schizonts in tail blood of Δ*smac*-infected mice (bottom right). (B) Representative distribution of sequestered schizonts in mice (and extracted organs) with synchronized infections of parasites that express luciferase under the schizont-specific *ama1* promoter as shown by measuring luciferase activity (RLU). WT-infected mice show the characteristic CD36-mediated schizont distribution in adipose tissue (belly), lungs, and spleen, whereas Δ*smac*-infected mice parasites show distribution throughout the body as shown by luciferase activity in the upper body (lungs and head), decreased sequestration in adipose tissue, and increased accumulation in the spleen (1, lungs; 2, spleen; 3, heart; 4, belly fat tissue). (C) Schizont loads in fat, spleen, and lungs, determined by measuring luciferase activity (RLU %), showing decreased loads in adipose tissue and increased loads in the spleen of mice infected with Δ*smac* ($n = 4$). Values are means ± SD.

activity in these organs (Fig. 3 B). In contrast, Δ*smac*-infected mice show a different pattern of luciferase activity with very low signals in adipose tissue of the belly and the pattern of luciferase activity in whole bodies of mice resemble the pattern observed in CD36$^{-/-}$ mice where the highest luciferase activity is observed in the spleen (Franke-Fayard et al., 2005). Analysis of the luciferase activity in organs confirmed the significant decrease ($P < 0.005$) of schizonts in the belly fat of Δ*smac*-infected mice, whereas the spleen of these mice showed a significant increase ($P < 0.005$) in schizonts compared with WT (Fig. 3, B and C). In whole body imaging, the head/breast area of Δ*smac*-infected mice show the strongest luminescence signals, which is indicative of schizonts in the peripheral circulation (Franke-Fayard et al., 2005) and differs from the more defined signals in lungs and adipose tissue observed in WT-infected mice.

To confirm that the changed sequestration pattern of schizonts is a result of the lack of SMAC expression and not of an unrelated genetic event in the Δ*smac* parasites, the Δ*smac3* parasites were complemented with a WT copy of *smac*. We first removed the drug-selectable marker, a fusion of the *hdhfr* and *yfcu* genes, from the genome of Δ*smac3* by negative selection resulting in parasite line Δ*smac3*$^{-sm}$ (Fig. S2). Subsequently, the *smac* gene was reintroduced into the *230p* locus of Δ*smac3*$^{-sm}$ under its own 5′- and 3′-UTR regions, resulting in parasite line Δ*smac3+smac*. Correct complementation of Δ*smac3*$^{-sm}$ parasites with a WT *smac* copy was shown by Southern analysis of digested DNA and Western analysis of SMAC expression in schizonts (Fig. S2). Comparison of schizont sequestration in cloned lines of Δ*smac3*$^{-sm}$ and Δ*smac3+smac* by real time in vivo imaging in live mice demonstrates a restored, normal pattern of sequestration of the schizonts of the complemented Δ*smac+smac* line with accumulation of schizonts in adipose tissue, lungs and spleen (Fig. S3).

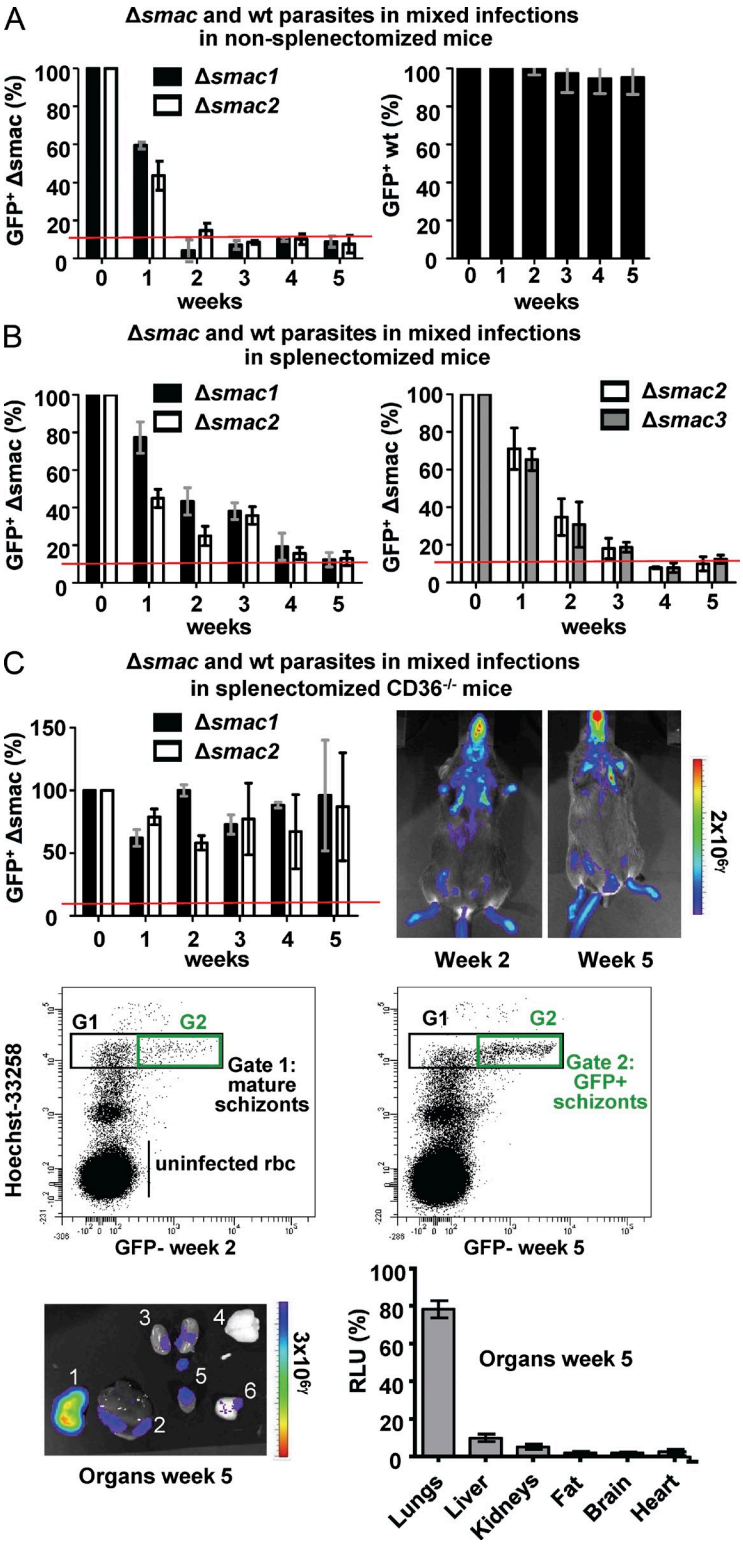

Figure 4. CD36-mediated schizont sequestration affects the growth rate of blood stage parasites. (A) In the GR assay, GFP-positive Δ*smac* parasites are no longer detectable after 2–3 wk (left) in nonsplenectomized mice ($n = 5$). The ratio between blood stages of Δ*smac* and WT is determined by FACS (C) and is the ratio between the number of GFP-expressing schizonts (Gate G2) to the total number of Hoechst-stained schizonts (Gate G1) in cultures of infected tail blood. Red line, the mean percentage of GFP-positive particles in G2 in tail blood of mice infected with non–GFP-expressing parasites. In the GR assay with two WT reference lines, cl15cy1 and WT-GFP-Luc$_{schiz}$, parasites of both lines, remain stably present during the 5-wk period (right). (B) In the GR assay, GFP-positive Δ*smac* parasites are no longer detectable after 4–5 wk in splenectomized mice ($n = 4$). (C) In the GR assay, GFP-positive Δ*smac* parasites remain present during the 5-wk period in splenectomized CD36$^{-/-}$ mice ($n = 4$; top left). During the 5-wk period, Δ*smac* parasites are detected in the peripheral blood circulation by in vivo imaging (top right) and by FACS analysis of GFP-positive Δ*smac* schizonts (middle). Quantification of parasite loads by in vivo imaging (expressed as RLU) of organs (week 5) shows low parasite loads in all organs except for the lungs (1, lungs; 2, liver; 3, kidneys; 4, brain; 5, heart; 6, belly fat tissue). Values are means ± SD.

Δ*smac* parasites have a reduced growth rate compared with WT parasites in nonsplenectomized and splenectomized mice

During the Δ*smac* cloning procedure in mice, we detected a reduction in blood stage multiplication rate compared with WT parasites (Table S4). Because the cell cycle of asexual Δ*smac* parasites is identical to WT parasites and because there was an increase in parasite load in the spleens of Δ*smac*-infected mice, we investigated if the reduced growth rate could be explained by spleen-mediated removal of circulating Δ*smac* schizonts. To determine the influence of the spleen on growth rate, we analyzed differences in growth rate between WT and Δ*smac* parasites by performing an in vivo growth rate assay (GR assay). In this assay, groups of mice are infected with equal numbers of WT and Δ*smac* parasites and these mixed infections are maintained by weekly passage of the infections into naive mice over a period of 5 wk. At regular intervals, the ratio between WT and Δ*smac* parasites is determined by FACS analysis. In this assay, one of the two lines in the mixed infections expresses GFP, which permits the determination of the ratio between the two lines by comparing the number of GFP-expressing blood parasites to the total number of Hoechst-stained parasites. Because the mixed infections are only maintained for short-term periods in mice (7 d) and parasites are weekly transferred to naive mice at a low (5–10%) parasitemia, it can be assumed that in these infections neither is there a competition for resources (e.g., host cells) between WT and Δ*smac* parasites nor do acquired immune responses influence parasite growth.

In nonsplenectomized mice, the initial (equal) ratio between WT and Δ*smac* parasites in the mixed infections changed rapidly and Δ*smac* parasites were no longer detectable after 2–3 wk (Fig. 4 A and Fig. S4). When the GR assay was performed by mixing two WT reference lines, the non–GFP-expressing cl15cy1 and WT-GFP-Luc$_{schiz}$, parasites

of both lines, remained stably present in mice during the growth period of 5 wk. These results demonstrate that the Δ*smac* parasites have a strongly reduced growth rate compared with WT parasites in nonsplenectomized mice. When the same GR assay was performed in splenectomized mice, a difference in growth rate between Δ*smac* and WT parasites was still observed. However, in mice without a spleen the rate at which the ratio between WT and Δ*smac* changed was slower, with Δ*smac* parasites becoming undetectable only after 4–5 wk compared with the 2–3 wk it took in infections in mice with a spleen (Fig. 4 B and Fig. S4 A). The change in the ratio of WT and Δ*smac* parasites in splenectomized mice was significantly different from that observed in mice with a spleen, as demonstrated by analysis of the relative change in ratio per week (= per passage) using linear mixed effects models (Table S6) and by survival analysis (Fig. S4 A). These results demonstrate that the spleen clearly contributes to the differences in growth between WT and Δ*smac* parasites. However, because Δ*smac* parasites are still lost from the mixed infections this would indicate that the spleen is not entirely responsible for the differences in growth between the nonsequestering Δ*smac* and the sequestering WT parasites.

Equal growth rates between nonsequestering Δ*smac* and sequestering WT parasites are achieved in splenectomized and nonsplenectomized mice that do not express CD36

Assuming that all growth characteristics, except for the CD36-mediated adherence, are the same between Δ*smac* and WT parasites, the reduced growth of Δ*smac* parasites in splenectomized mice implies that CD36-mediated adherence has, in addition to permitting schizonts to avoid removal by the spleen, other benefits to parasite survival. To test this hypothesis, we performed the GR assay in mice that not only had their spleen removed but also did not express CD36 (CD36$^{-/-}$ mice). In splenectomized CD36$^{-/-}$ mice, both WT and Δ*smac* parasites remained present in mice during the growth period of 5 wk (Fig. 4 C and Table S6). The presence of Δ*smac* schizonts after 5 wk in the splenectomized CD36$^{-/-}$ mice was also demonstrated by in vivo imaging of schizonts. Δ*smac* schizonts are mainly found in the blood circulation and in the lungs (Fig. 4 C; and Fig. S4, B and C). No clear luciferase activity is detected in the liver, suggesting that in the absence of the spleen, the liver has little or no role in schizont trapping or removal. As an additional proof that absence of CD36-mediated adherence is responsible for the reduced growth rate of Δ*smac* parasites, we performed GR assays in CD36$^{-/-}$ mice where the spleen had not been removed. In these mice, we also observe that both WT and Δ*smac* parasites persist in similar ratios throughout the course of the 5-wk experiment (Fig. S4 C and Table S6). Therefore, in CD36$^{-/-}$ mice, where parasites of both lines are unable to adhere to CD36, WT and Δ*smac* parasites have similar growth rates.

DISCUSSION

Irbc of different (rodent, nonhuman primate, and human) *Plasmodium* species sequester in host arterioles, capillaries, and venules mediated by a cytoadherence to endothelial cells. The current paradigm states that cytoadherence is beneficial for the parasite, as cytoadherence-based sequestration prevents mature irbc from being retained and cleared by the spleen (Miller et al., 1994; Sherman et al., 2003; Buffet et al., 2011). Many questions regarding the role of sequestration remain unanswered—both the pathogenic consequences and its effect on parasite growth—because experimental studies addressing these questions are difficult to perform in humans or in nonhuman primates. Although experimental models of cytoadherence in nonhuman primates do exist and have been instrumental in highlighting a possible role of the spleen in modulating antigenic expression (Barnwell et al., 1982, 1983), the impact of sequestration on parasite growth and pathology is unknown, in part as a result of the absence of the transgenics available in rodents (e.g., the CD36$^{-/-}$ mice used in this study). In this paper, we provide direct evidence, using a rodent model of malaria, that sequestration benefits the growth rate of blood stage parasites. Blood stages of the mutant parasite Δ*smac* with a reduced sequestration phenotype have significantly lower growth rates in vivo when compared with sequestering blood stages of WT parasites. When placed in the context of the prevailing hypothesis for sequestration, i.e., avoidance of spleen removal, it is unexpected that the reduced growth rate of Δ*smac* cannot be explained exclusively by removal of irbc by the spleen. In splenectomized mice, Δ*smac* parasites were still at a growth disadvantage compared with WT parasites and the growth rate of Δ*smac* parasites was only comparable to that of WT parasites in infections of splenectomized CD36$^{-/-}$ mice, where WT parasites are also unable to sequester via CD36 adherence. The reduced growth rate in splenectomized mice might be explained by clearance of circulating Δ*smac* schizonts by other organs in the absence of the spleen, for example by the liver (Quinn and Wyler, 1979; Sayles et al., 1991; Moore et al., 2008). In splenectomized CD36$^{-/-}$ mice, however, we found no evidence for an accumulation of schizonts in the liver, although it cannot be excluded that, unlike in the spleen, irbc are more rapidly destroyed in the liver which hampered detection by imaging.

The observations of the reduced growth of nonsequestering Δ*smac* parasites in splenectomized mice support the hypothesis that irbc sequestration may confer advantages to parasite growth in addition to avoidance of spleen removal. For example it has been proposed that sequestration place the irbc in a microenvironment that either favors growth and multiplication of the parasite (Sherman et al., 2003; Krücken et al., 2005) or that CD36-mediated adherence modulates immune-effector mechanisms that enhance parasite survival (Urban et al., 1999; Serghides and Kain, 2001; Patel et al., 2004; Terrazas et al., 2010). It is possible that the reduced growth rate of the Δsmac parasites in our experiments can be explained by a modulation of immune responses because acquired immune responses can affect both growth and tissue sequestration. However, because the growth competition experiments between WT and Δsmac parasites were performed using short-term infections in naive mice, it is likely

that the effect of acquired immune responses is limited. During the infection period of the first 6–7 d, WT *P. berghei* parasites show a very stable multiplication rate of ∼10 per 24 h (Spaccapelo et al., 2010). Clearly, it would be of great interest to further examine in detail the contribution of innate and adaptive immune responses on reducing parasite growth rate, in particular the role of the spleen in removing parasites that do not sequester. Analyses of growth rate in splenectomized RAG-deficient or SCID mice, or using rodent parasites that induce long-lasting infections, e.g., *Plasmodium chabaudi* which is known to sequester (Mota et al., 2000), may help to unravel the importance of acquired immunity for both the rate of multiplication and changes in sequestration patterns.

Compared with other nonhuman malaria parasites, *P. berghei ANKA* is the best exploited *Plasmodium* model with respect to investigations of sequestration of schizonts. It has been shown that *P. berghei* ANKA parasites demonstrate a clear sequestration phenotype with irbc disappearing from the peripheral circulation at the start of schizogony (Franke-Fayard et al., 2005, 2010). These schizont-infected rbc accumulate in microvasculature of adipose tissue and lungs as a result of adherence to CD36. The role of CD36 as a major receptor for the adherence of *P. falciparum* irbc to endothelial cells is well established (Sherman et al., 2003; Bull et al., 2005; Rowe et al., 2009). The evidence for the involvement of CD36 in irbc sequestration in other rodent and primate *Plasmodium* species (Aikawa et al., 1992; Mota et al., 2000) suggests that CD36-mediated sequestration is an ancient feature of mammalian *Plasmodium* species, presumably performing the same role across the genus. Irrespective of the putative functions of CD36-mediated sequestration, it is evident that the parasite proteins responsible for binding to CD36 are not the same in different *Plasmodium* species. The PfEMP1 proteins that are responsible for *Plasmodium falciparum* CD36 adherence are absent in the rodent malaria parasites (Hall et al., 2005) and *Plasmodium knowlesi* (Pain et al., 2008), a species which is known to sequester. In addition, we found that the specific domains of PfEMP1 that mediate binding to CD36, the so-called CIDR domains, are not present in proteins of *P. berghei ANKA*. In our proteome/gene deletion screen, we identified a *P. berghei ANKA* mutant that lacks expression of SMAC, a small protein containing a signal anchor, a transmembrane domain, and a predicted PEXEL. In peripheral blood of mice infected with this mutant, schizonts were readily observed associated with a strong reduction of irbc sequestration in adipose tissue. However, our observations on the localization of SMAC suggest that SMAC does not bind directly to CD36. SMAC is exported out of the parasite into the cytoplasm of the irbc, but there is no evidence that this protein translocates onto the surface of the rbc. However, the localization of SMAC is based on the detection of SMAC by antibodies and detection of mCherry-SMAC and we have been unable to detect SMAC in irbc by immunoelectron microscopy. It therefore remains possible that a low amount of SMAC is expressed on the irbc surface but is below detectable limits or that SMAC expression on the erythrocyte surface was compromised by the mCherry tag. Clearly, further studies are required to better understand the function of SMAC and its role in irbc attachment to host receptors.

Interestingly, in infections with Δ*smac* mutants, despite the strong reduction in CD36-mediated sequestration in adipose tissue, the accumulation of irbc in the lungs appears to be less reduced. Because the lungs are blood-rich organs and no organ perfusion was used in our experiments, the high parasite loads might be explained by the presence of nonsequestered schizonts. However, it is also possible that *P. berghei ANKA* sequestration is a process that is dependent on a complex of multiple parasite ligands and that the composition of the complex affects binding to endothelium of the lungs and adipose tissue in a different way. Therefore, the absence of SMAC on sequestration in lungs and adipose tissue might be the result of SMAC, or SMAC-associated proteins, being lost or redistributed in the complex resulting in compromised binding in certain organs and not in others. To identify additional parasite proteins that are involved in binding to CD36 we have knocked out several other genes encoding putative exported proteins in *P. berghei ANKA* including members of the *bir*, *pb-fam-1*, and *pb-fam-3* multigene families and proteins that we identified in coprecipitation studies using mCherry-tagged SMAC (this study and unpublished results). So far we have been unable to identify additional mutants where infections result in an increased numbers of schizonts in the peripheral circulation and currently all mutants tested exhibit the WT phenotype (i.e., CD36-mediated sequestration).

Combined, our studies show a clear benefit of sequestration on parasite infections, demonstrated by higher growth rates of sequestering parasites compared with the nonsequestering Δ*smac* parasites. A cautious extrapolation from rodent models to human infections, based on impaired growth rates of nonsequestered parasites, support strategies that aim to reduce *P. falciparum* severe pathology by interfering with irbc sequestration (Rowe et al., 2009; Avril et al., 2010; John et al., 2010). The results of our studies indicate that in addition to directly reducing parasite loads in critical tissues such as the brain, anti-adhesion adjunctive therapies may enhance irbc removal by the spleen and prevent irbc accumulating at sites favorable to parasite growth and multiplication. However, despite the strong association between sequestered *P. falciparum* parasites in the brain and cerebral complications, the relative contribution of CD36-mediated sequestration to severe pathology is not well understood. Studies on irbc-CD36 binding and pathology in humans are often contradictory, where a decrease in CD36 adherence has been correlated with either no effect, an increase, or a decrease in disease severity (Rogerson et al., 1999; Aitman et al., 2000; Serghides and Kain, 2001; Patel et al., 2004). Most of what we know about *P. falciparum* adherence of irbc to host cell receptors has mainly been derived from binding assay studies performed in vitro or from postmortem samples, and the relative contribution that adherence to different receptor in different organs has to severe pathology has yet to be resolved. Such studies would benefit from the availability of inhibitors that would interfere with

sequestration by targeting only specific receptors. The characterization and the genetic modification of *P. berghei ANKA* ligands involved in binding to the different host receptors, as shown in this study, might offer novel possibilities for the development of small-animal models to analyze sequestration properties of *P. falciparum* ligands that have hitherto only been examined in vitro. For instance this could be performed by substituting *P. berghei ANKA* ligands with *P. falciparum* PfEMP1 proteins or domains. Using in vivo imaging in conjunction with such falciparumized *P. berghei ANKA* parasites in mice expressing human receptors (e.g., human ICAM-1; Dufresne and Gromeier, 2004) may create an in vivo screening system for testing inhibitors that block *P. falciparum* sequestration. We believe that the *P. berghei ANKA* mutant Δ*smac*, in which irbc CD36-mediated sequestration is removed, would make an excellent tool for introducing domains of *P. falciparum* ligands using *P. berghei* proteins that are still transported onto the irbc surface by a SMAC-independent pathway. This would create an in vivo model for screening of vaccines/small molecule inhibitors for their efficacy to interfere with adherence of *P. falciparum* ligands to host receptors.

MATERIALS AND METHODS

Experimental animals and reference *P. berghei* ANKA lines. Female C57BL/6 and Swiss OF1 mice (6–8 wk; Charles River), female Wistar rats (6 wk), and CD36-null C57BL/6 ($CD36^{-/-}$) mice (female, 5–8 wk old; Franke-Fayard et al., 2005) were used. All animal experiments were performed after a positive recommendation of the Animal Experiments Committee of the LUMC (ADEC) was issued to the licensee. The Animal Experiment Committees are governed by section 18 of the Experiments on Animals Act and are registered by the Dutch Inspectorate for Health, Protection, and Veterinary Public Health, which is part of the Ministry of Health, Welfare and Sport. The Dutch Experiments on Animal Act is established under European guidelines (EU directive no. 86/609/EEC regarding the Protection of Animals used for Experimental and Other Scientific Purposes).

Two reference *P. berghei* ANKA parasite lines were used: line cl15cy1 (WT; Janse et al., 2006) and reporter line 1037cl1 (WT-GFP-Luc_{schiz}; mutant RMgm-32; www.pberghei.eu). This reporter line contains the fusion gene *gfp-luc* gene under control of the schizont-specific *ama1* promoter integrated into the silent *230p* gene locus (PBANKA_030600), and it does not contain a drug-selectable marker (Spaccapelo et al., 2010).

Proteome analyses of membranes of irbc. Synchronized infections of *P. berghei ANKA* in Wistar rats were established by intravenous injection of cultured and purified mature schizonts as previously described (Janse and Waters, 1995). In these animals, merozoites invade within 3–4 h after injection of the schizonts, giving rise to synchronized infections. Infected heart blood with a parasitemia of 1–3% and containing ring forms is collected at 4 h after schizont injection in complete RPMI1640 culture medium. After removal of leucocytes using Plasmodipur leukocyte filters (Euro-diagnostica B.V.; Janse and Waters, 1995), parasites were cultured for a period of 22 h using standardized in vitro culture conditions (Janse et al., 2006), allowing the ring forms to develop into schizonts. At 22 h, irbc containing immature and mature schizonts were collected by Nycodenz density gradient centrifugation (Janse et al., 2006). Two different methods were used to collect membrane fractions of the Nyodenz-purified schizonts, i.e. the HL and the SS method.

For the HL method (Pasini et al., 2006) $2–3 \times 10^8$ irbc were washed three times in PBS buffer (pH 7.4) at 4^0C. Infected rbc were then resuspended in 50 ml ice-cold 5 mM phosphate buffer (pH 8) for lysis of the rbc, followed by centrifugation for at 4°C. The supernatant was collected and washed five times (20 min, 9,000 *g*) until the supernatant appeared colorless. Centrifugation of the collected supernatant was then increased to 20,000 *g* to pellet the membranes and washing of the membrane pellet was repeated until the ghost membranes appeared yellow-whitish. Membranes were stored at −80°C.

For the SS method $2–3 \times 10^8$ irbc were washed three times in PBS buffer (pH 7.4) at 4^0C. Pelleted irbc (400 *g*, 5 min) were subsequently resuspended in an equal volume of PBS to which 1.5 mg Trypsin (TRTPCK; Worthington) was added. The suspension was incubated for 50 min at RT, after which irbc were pelleted by centrifugation (5 min, 800 *g*). The supernatant was collected, centrifuged once more for 15 min, (25,000 *g*), and stored at −80°C. Before LC-MS/MS analysis, the supernatant was reduced and alkylated by adding 1 µg DTT per 50 µg protein followed by incubation at room temperature for 30 min and samples were then supplemented with 5 µg iodoacetamide per 50 µg protein for 20 min at room temperature.

The protein content of the different HL and SS samples was measured using the MicroBCA assay using BSA as a standard (Thermo Fisher Scientific) according to the manufacturers' instructions. 10 µl of a 10% (wt/vol) lithium dodecylsulfate solution was added to 10 µl HL samples, the mixture was incubated for 10 min at 70°C, and 10 µl of the mixture was run on a precast 4–12% polyacrylamide gel (NuPAGE; Invitrogen) in MOPS buffer supplemented with 0.025% (vol/vol) reducing agent (Invitrogen) in the inner chamber to prevent sample reoxidation. SDS-PAGE track lengths (top to tracking dye) averaged 7 cm and lanes were cut into 10 slices, which were individually digested with trypsin as previously reported (Wilm et al., 1996). Aliquots of trypsin-digested material from both the HL and SS samples were diluted 1:5 with 0.5% glacial acidic acid, 1% trifluoroacetic acid (vol/vol). Samples were loaded on a stage tip (Rappsilber et al., 2003) to desalt and stored for maximally 12 h at 4°C. Peptides were eluted with 3× 10 µl buffer B (80% acetonitrile, 20% MilliQ water, 0.5% glacial acidic acid [vol/vol]) directly into 96-well plates (ABgene, AB-0800), which were centrifuged under vacuum until volumes were 4–6 µl. Subsequently, buffer A (containing 0.3% trifluoroacetic acid) was added to the wells to a final volume of 10 µl.

The trypsin digested from both HL and SS samples were analyzed by capillary liquid chromatography coupled online with LC-MS/MS using an 1100 series system (Agilent Technologies) and an Orbitrap Mass Spectrometer (three runs; Thermo Fisher Scientific). Samples of 3 µg protein were separated by reverse-phase chromatography (3 µm Reposil C18, 75 µm × 12 cm column) using a gradient of 98% MS Buffer A (0.5% glacial acidic acid, vol/vol) and 2% MS Buffer B (80% acetonitrile and 0.5% glacial acidic acid, vol/vol) at a 0.5 µl/min flow rate. After 24 min, the flow rate was decreased to 0.25 µl/min and the amount of buffer B was increased by the following steps: 7% at 27 min, 13% at 35 min, 33% at 95 min, 50% at 112 min, 60% at 117 min, and 80% at 123 min. Eluted peptides were ionized to charge states 1+, 2+, or higher by the electrospray source and peptides that were at least doubly charged were analyzed in data-dependent MS experiments with dynamic exclusion. The MS method used is based on the previously published "three most intense ions" method (Olsen and Mann, 2004) but was modified to pick the 10 most intense ions instead of only three.

Acquired MS/MS spectra were searched against a decoy database composed of the nonredundant International Protein Index (IPI) mouse sequence database (Kersey et al., 2004) and the *P. berghei ANKA* Sanger Database using the Mascot software (Hirosawa et al., 1993). The decoy database was used to determine levels of false positive peptide identifications. The estimated rate of peptide false positives was 0.5% for the HL samples and 0.6–0.7% for the SS samples. Search parameters for initial peptide and fragment mass tolerance were ± 5 ppm and ± 0.6 D, respectively, with allowance made for one missed trypsin cleavage, fixed modification of cysteine through carbamidomethylation and acetylation, and methionine oxidation as variable modification. Only fully tryptic peptide matches were allowed.

Validation of the identified proteins was performed using MSQuant, which is an open source software package (developed by the Mann laboratory, http://msquant.sourceforge.net), enabling manual score and spectrum evaluation of each peptide that led to the identification of a protein. Stringent protein identification criteria were imposed: each protein required minimally a unique, 7-aa peptide with a Mascot score >35 (corresponding to 99.9% identification confidence) and an MS/MS spectrum featuring a continuous

series of at least three y-ions in the area ≥y5 or a continuous series of 3 y- or b-ions. Protein identification by a single peptide was only allowed if the protein was identified in at least two runs.

The information on *Plasmodium* genes/proteins available PlasmoDB and GeneDB were used for annotation and to analyze the presence of specific protein features such as transmembrane domains, GPI anchors, and signal sequences. HMM analysis of proteins was performed with HMMer v2.3.2 (obtained from http://hmmer.janelia.org and run locally). All sequences used for building HMMs (PEXEL and CIDR/DBL) were aligned in Clustal X (using default alignment parameters). HMMs for CIDR and DBL domain searches were built and calibrated from previously defined *P. falciparum Pfemp1* sequences (Smith et al., 2000) obtained from National Center for Biotechnology Information. HMM searches (default settings, except E = 10) were performed against all predicted *P. falciparum* and *P. berghei ANKA* proteins (www.plasmodb.org; 2006; release 5.2). In Table S1, more details of the HMM searches are given. An HMM for PEXEL searches was built and calibrated from previously predicted PEXEL sequences (Marti et al., 2004). HMM searches (default settings, except E = 900) were performed against all predicted *P. berghei ANKA* proteins (www.genedb.org January 2010 Assembly and as implemented in www.plasmodb.org; release 7.0, 2010). To reduce the number of false positives, all *P. berghei ANKA* sequences were truncated before HMM searches to include only the first 100 aa in the HMM analysis. A region of 100 aa is consistent with the location of PEXEL motifs (Hiss et al., 2008). In Table S1, more details of the HMM searches are given. In total, 438 proteins were retrieved with the PEXEL HMM search (Table S1). Only HMM scores of ≥2 were included because the majority of previously predicted exported *P. berghei ANKA* proteins retrieved from the HMM search (38 of 49 proteins; 78%) had a value of ≥2.

Proteome analysis of P. berghei ANKA merozoites. Purified mature schizonts of *P. berghei* ANKA (cl15cy1) were isolated using Nycodenz density gradient centrifugation as described in Proteome analyses of membranes of irbc. Free, viable merozoites were harvested by membrane filtration. In brief, schizonts were resuspended in culture medium to a 5–10% cell suspension in a total volume of 10–20 ml and the solution transferred to a culture chamber ultra-filtration cell (Amicon 8010) fitted with a 2-µm pore-size polycarbonate membrane (Nuclepore Corp). The suspension was passed through the filter by applying sufficient N_2 gas pressure while the cells were vigorously stirred using the stirrer contained within the filtration unit. Free merozoites were contained in the effluent and harvested by centrifugation (400 *g*, 8 min). Numbers of free merozoites were determined by counting in a Bürker-Türk counting chamber using phase-contrast microscopy. Mass spectrometry analysis performed on 10^9 merozoites was conducted as previously described (Khan et al., 2005). In brief, protein mixtures of all samples were extracted in SDS-PAGE (SDS-PAGE) loading buffer and separated into 10 fractions by electrophoresis on a 10% PAGE gel. Proteins were treated with dithiothreitol (DTT) and iodoacetamide and in-gel digested by trypsin. Essentially, peptide mixtures were loaded onto 100 µm ID columns, packed with 3 µm C18 particles (Vydac), and electrosprayed into a quadruple time-of-flight mass spectrometer (QSTAR; Sciex-Applied Biosystems). Fragment ion spectra were recorded using information-dependent acquisition and duty-cycle enhancement. To acquire MS/MS spectra of the peptides, samples were measured at least three times with exclusion lists. Malaria proteins were identified by searching combined protein databases of *P. berghei ANKA*, *Mus musculus*, and human IPI using Mascot (Matrix Science). Stringent protein identification criteria were imposed: each protein required minimally a unique, 7-aa peptide with a Mascot score >30 (corresponding to 99.9% identification confidence). Protein identification by a single peptide was only allowed if the protein was identified in at least two runs. The information on the 781 *P. berghei ANKA* merozoite proteins, and corresponding peptides, has been deposited with PlasmoDB.

Generation of transgenic/mutant *P. berghei* ANKA parasites and parasites lacking expression of SMAC. Transfection of *P. berghei ANKA*, selection, and cloning of transgenic and mutant parasite lines was performed as previously described (Janse et al., 2006). Correct integration of the DNA constructs was determined by PCR and/or Southern blot analysis of digested genomic DNA or chromosomes separated by pulse-field gel (PFG) electrophoresis. Blots were hybridized with the following probes: 3′UTR *dhfr/ts* of *P. berghei ANKA* and *smac* probes (for details of the primers refer to Table S5).

Two general gene targeting DNA constructs pL0001 or pL0037 (available from MR4, www.mr4.org) were used to generate constructs to disrupt the genes selected from the proteome analyses. These constructs are aimed at targeted gene disruption by double crossover homologous recombination. Sequences of the open reading frame (ORF) and UTR regions of the selected genes were retrieved from PlasmoDB and GeneDB. To replace the ORF of the target genes with the selection cassette containing the pyrimethamine-resistant *dhfr/ts* of *Toxoplasma gondii*, the 5′ and 3′ flanking regions of the ORF were cloned up- and downstream of the selection cassette of pL0001 or pL0037. The primers used to amplify the target regions are listed in Table S5 A. For each gene, at least two independent transfection experiments were performed using *P. berghei ANKA* parasites of reference line 1037cl1.

Parasites lacking expression of SMAC (Δ*smac*) were generated using DNA construct pL1351 or pL1386. To generate pL1351, the 5′UTR region of *smac* was amplified (*Asp*718/*Hind*III; Table S5, primers 3423–3424) and cloned in pL0001. Subsequently, the 3′UTR region was cloned as an *Eco*RI–*Xba*I fragment (Table S5, primers 3425–3426) to obtain pL1351. Plasmid pL1351 was linearized using *Asp*718, *Xba*I, and *Sca*I and transfected into parasites of reference WT-GFP-Luc_{schiz}. Selection and cloning of transfected parasites in two independent experiments resulted in the generation of the lines 1119cl1 (Δ*smac1*) and 1160cl7 (Δ*smac2*). To obtain a drug-selectable marker free Δ*smac* parasites line, the positive *T. gondii dhfr/ts* selectable marker of pL1351 was replaced with the drug selection cassette of pL0037 (*Hind*III–*Eco*RI fragment) that contains a fusion of the positive selectable marker, *hdhfr*, and the negative selectable marker *yfcu* (Braks et al., 2006). This construct, pL1386, was used to transfect parasites of reference line WT-GFP-Luc_{schiz} and positive selection with pyrimethamine followed by cloning of parasites resulted in the generation of line 1242cl5 (Δ*smac3*). To select for parasites which had removed the selectable marker cassette, we applied negative selection with 5-fluorocytosine (5-FC) as previously described (Braks et al., 2006). Four mice infected with Δ*smac3* were treated with 5-FC starting at a parasitemia of 0.1–0.5% with a daily single dose of 0.5 ml of 20 mg/ml drug/day for a period of 4 d. Resistant parasites were collected between days 5 and 7 after initiation of the 5-FC treatment, and the genotype was analyzed by diagnostic Southern analysis to confirm removal of the drug-selectable marker *hdfr-yfcu* by a recombination event between the two 3′-UTR *dhfr* sequences present in pL1386. Parasites from one of the four mice (mouse 2) that had been treated with 5-FC were cloned resulting in line 1242cl5m2cl1 (Δ*smac3*$^{-sm}$). This line was used for complementation of Δ*smac* parasites with a WT copy of *smac* (see the subsequent section).

To generate transgenic parasites that express mCherry under control of the 5′- and 3′-UTR regions of *smac*, the 5′- and 3′-UTR regions of the mCherry expression cassette of pL0017-mCherry (Graewe et al., 2009) were exchanged by the 5′- and 3′-UTRs of *smac* (*Eco*RV–*Bam*HI), resulting in pL1378 (The 5′- and 3′-UTR were PCR amplified using the primer pairs 3733/3734 and 5777/5778: Table S5). This construct was used to transfect parasites of the reference line cl15cy1. Selection of parasites containing the construct integrated into the *c/d-ssu-rrna* locus resulted in transgenic line $smac_{5'UTR}$-mCherry. To generate transgenic parasites expressing SMAC that is C-terminally tagged with mCherry, construct pL1419 was generated. First the *mCherry* gene of pL0017-mCherry (Graewe et al., 2009) was cloned into pL0017eGFPcam (*Bam*HI–*Xba*I). Next, the mCherry expression cassette of pL0017mCherrycam was subcloned in pBluescript (*Bam*HI–*Eco*RI) and then cloned (*Hind*III–*Eco*RI) into pL0001 to obtain the mCherry-tagging vector. Finally, the *smac* targeting region (Table S5, primers 3774–3775, *Spe*I–BglII) was cloned into the mCherry-tagging plasmid cut with *Spe*I–*Bam*HI to obtain pL1419. This construct was used to transfect parasites of the reference line cl15cy1. Selection and cloning of parasites containing the construct integrated into the *smac* locus resulted in transgenic line smac::mCherry.

Complementation of Δsmac with a WT copy of smac. To complement Δ*smac3*$^{-sm}$ with a WT copy of *smac* the construct pL1649 was generated. Two integration regions of the target locus *230p* (PBANKA_030660) gene were cloned into pL0035 (Braks et al., 2006) using primers 3739–3698, *Hind*III–*Not*I and 3786–3787, *Eco*RV–*Kpn*I (Table S5) to create plasmid 230pFCU. The *230p* gene is a silent locus that is generally used for integration of transgenes in *P. berghei ANKA*. The mCherry gene of pL1378 (see the previous section) was exchanged for the ORF of the *smac* gene (Table, S5, primers 5505–5506) and, finally, the *smac* expression cassette of pL1378 was cloned as *Eco*RV–*Kpn*I fragment into 230pFCU to create pL1649. This construct was used to transfect Δ*smac3*$^{-sm}$ parasites. Selection and cloning of parasites containing the construct integrated into the *230p* locus resulted in transgenic line 1758cl5 (Δ*smac*+smac).

Analysis of smac expression by Northern and Western analyses and fluorescence microscopy. Transcription of *smac* was determined by Northern analysis of RNA obtained from blood stages of synchronous in vivo infections using a probe specific to the 5′UTR of *smac* (Table S5, primers 3423–3424). SMAC expression was analyzed by Western analysis using polyclonal antibodies against a SMAC peptide (CTHGQYKYHRNNVYT-amide) that were raised in rabbits by Biogenes (www.biogenes.de). After three boosts, serum was collected and used at a 1:1,000 dilution as the primary antibody for Western blotting. As a control for protein loading, a mouse monoclonal antibody probe recognizing *P. berghei ANKA* HSP70 (PBANKA_071190) was used.

For analysis of mCherry expression of the transgenic lines, live parasites were collected in PBS and were examined by microscopy using a DMR fluorescent microscope (Leica) with standard FITC and Texas Red filters. Parasites nuclei were labeled by staining with Hoechst 33258 (Sigma-Aldrich) and rbc surface membranes were stained with the anti–mouse TER-119-FITC–labeled antibody (eBioscience). In brief, erythrocytes were stained with TER-119-FITC antibody (1:100) and Hoechst-33258 (2 µmol/liter) at room temperature for 30 min and washed with 500 µl RPMI-1640 medium (400 *g*; 2 min). Pelleted cells (400 *g*, 2 min) were resuspended in RPMI-1640 medium and images were recorded with the digital camera CoolSNAP HQ^2 (Photometrics) and processed with the ColorProc software (Tanke et al., 1999).

Determination of growth and multiplication of asexual blood stages. The in vivo multiplication rate of asexual blood stages was determined during the cloning procedure as previously described (Spaccapelo et al., 2010). The percentage of infected erythrocytes in Swiss mice (8 wk old) injected with a single parasite was determined at days 8–11 in Giemsa-stained blood films. The mean asexual multiplication rate per 24 h was then calculated assuming a total of 1.2×10^{10} erythrocytes/mouse (2 ml of blood). The percentage of infected erythrocytes in mice infected with reference lines of the *P. berghei* ANKA strain consistently ranged between 0.5 and 2% at day 8 after infection, resulting in a mean multiplication rate of 10 per 24 h (Janse et al., 2003; Spaccapelo et al., 2010). Such an analysis is a sensitive method to quantify (differences in) growth rates during the early phase of in vivo infections when the availability of suitable host cells (reticulocytes) is not a limiting factor (Spaccapelo et al., 2010).

For determination of the number of merozoites per schizont, infected blood samples containing schizonts were stained with the DNA-specific, fluorescent dye Hoechst 33258 and analyzed by flow cytometry as described by Spaccapelo et al. (2010). Infected blood (1–3% parasitemia) is collected from Wistar rats by heart puncture and cultured overnight under standard culture conditions for collecting *P. berghei ANKA* schizonts (Janse et al., 2006). After overnight culture, the infected erythrocytes were separated from uninfected cells by Nycodenz density centrifugation and fixed in 0.25 (vol/vol) glutaraldehyde solution in PBS. These samples were stained with Hoechst-33258 (2 µmol/liter) for 1 h at 37°C and analyzed with a FACScan (LSR II; BD). No gate was set in the forward/sideward scatter for size selection of erythrocytes to include the small, free merozoites for analysis. The fluorescence intensity of a total of 50,000 cells per sample was measured, and data analysis was performed using CellQuest software (BD). The mean fluorescence intensity of free merozoites (first peak, G1, in the fluorescence histograms in Fig. 2) was proportional to the haploid DNA value (Janse et al., 2003) and is set at 1. The number of merozoites per schizont was calculated by dividing the mean fluorescence intensity of mature schizonts (peaks G3; Fig. 2) by the mean fluorescence intensity of the merozoites.

The length of the asexual blood stage was determined in standard short-term cultures of synchronized *P. berghei ANKA* blood stages as previously described (Janse et al., 2003; Spaccapelo et al., 2010). In brief, cultured and purified schizonts, collected as described in the previous paragraph, were injected into the tail veins of mice. In these animals, merozoites invade within 4 h after injection of the schizonts, giving rise to synchronized in vivo infections with a parasitemia of 0.5–3%, containing mainly (>90%) ring form parasites. At 2–4 h after injection of the schizonts, infected blood was collected from the mice by heart puncture and cultured in vitro under standard culture conditions for a period of 24 h at 37°C. At fixed time points after the start of the cultures, 1-ml samples were collected for analysis of the cell cycle by flow cytometry. Cells, fixed in 0.25 (vol/vol) glutaraldehyde solution in PBS, were stained with Hoechst-33258 (2 µmol/liter) for 1 h at 37°C and analyzed with a FACScan (LSR II). The fluorescence intensity and size (forward/sideward scatter) of a total of 50,000 cells per sample were measured, and data analysis was performed using CellQuest software (BD). No gate was set in the forward/sideward scatter for size selection of erythrocytes to include the small, free merozoites for analysis. The fluorescence intensity of infected erythrocytes was proportional to the DNA content of the parasites. The start of schizogony (the length of the growth, G1, phase of trophozoites) is defined as the time point (hours post invasion [hpi]) at which the percentage of cells with more than the diploid DNA content had increased >5% compared with that at the previous time point (Spaccapelo et al., 2010). The time points at which the first schizonts are mature (end of the DNA synthesis/mitosis, S/M, phase) is defined as the time point (hpi) at which the percentage of free merozoites (Gate G1, Fig. 2) had increased >5% compared with the previous time point (Spaccapelo et al., 2010).

FACS and bioluminescence analysis of schizonts in the peripheral blood circulation. The presence of schizonts in the peripheral blood circulation was determined in tail blood of mice with synchronized infections. For FACS analysis, 10 µl of tail blood infected with parasites expressing GFP-Luciferase (under control of the schizont-specific *ama-1* promoter) was collected at 22 hpi in 1 ml of complete culture medium, stained with Hoechst-33258 (2 µmol/liter) for 1 h at 37°C, and analyzed for both Hoechst and GFP fluorescence with a FACScan (LSR II). In the samples, the total number of schizonts (Gate G1: parasites with >2N DNA content) and mature schizonts (Gate G2: parasites expressing GFP) was determined (see Fig. 3 A for gates G1 and G2). For quantification of bioluminescence (luciferase activity), 10 µl of tail blood infected with parasites expressing GFP-Luciferase (under control of the schizont-specific *ama-1* promoter) was collected at 22 hpi in heparinized tubes and frozen in Eppendorf tubes at −20^{0}C until analysis. Before the analysis, the samples were thawed at room temperature and processed according to the protocol of Promega Luciferase Assay system. Luminescence spectra of the samples were measured by using a multilabel plate reader (Wallac 1420 Workstation with VICTOR^{2}V software; PerkinElmer).

Real-time in vivo imaging of schizont sequestration in whole bodies of live mice and dissected organs. Sequestration of schizonts in whole bodies of live mice and isolated organs was visualized through imaging of luciferase-expressing, transgenic parasites with an intensified charge-coupled device photon counting video camera of the in vivo imaging system (IVIS 100; Caliper Life Sciences) as described previously (Franke-Fayard et al., 2005, 2006). Sequestration patterns were monitored in mice with synchronized infections. Synchronized infections (1–3% parasitemia) were established by injection of cultured, purified schizonts as described in Determination of growth and multiplication of asexual blood stages. Imaging of schizonts was performed between 15 and 24 h after infection of the mice. Imaging of individual organs, obtained by dissection from animals at 21–23 h after infection, was done as described previously (Franke-Fayard et al.,

2005, 2006). Whole body images were also used to measure the percentage of schizont load in fat tissue. For the belly fat measurement, two regions of interest (ROI) were defined: one on the left part of the belly fat—to avoid measurement of luminescence from the spleen—and one on the total mouse (Fig. S3). Imaging data were analyzed by using the programs LIVING IMAGE 4.2 (Caliper Life Sciences).

In vivo GR assay in (non) splenectomized mice. To detect growth differences during blood-stage development between WT and Δ*smac* parasites, a GR assay was used as described by Janse et al. (2003). In the GR assay, groups of four to five mice were infected with equal numbers of blood stage parasite of two different parasite lines, one of which expresses GFP under the control of the *ama-1* promoter as a reporter for FACS analysis. At the start of the GR assay, mice were infected with an intraperitoneal inoculum of a mixture of 10^4 blood stages of each line. The infections in all mice were maintained by weekly passage of 10^4 blood stages to naive mice for a period of 5 wk. At regular intervals, the ratio between parasites of the two different lines was determined by FACS analysis. For FACS analysis, tail blood of mice containing mixed infections was collected (10 µl of tail blood in 1 ml of complete culture medium) and cultured overnight under standard in vitro culture conditions to allow the blood stage parasites to mature into schizonts. These cultures were stained with Hoechst-33258 (2 µmol/liter) for 1 h at 37°C and analyzed with a FACScan (LSR II). The ratio between blood stages of the two lines was determined by calculation of the number of GFP-expressing mature schizonts (Gate 2) to the total number of Hoechst-stained mature schizonts (Gate 1). See Fig. 4 C for the gates G1 and G2. The fluorescence intensity of a total of 50,000 cells per sample was measured, and data analysis was performed using CellQuest software (BD).

The data of the in vivo growth rate experiments were evaluated with survival analysis. The time until the proportion of GFP-positive Δ*smac* parasites became less than the lower threshold was evaluated using log-rank tests and data are presented as Kaplan-Meier curves. The lower threshold (14.4) was defined as the mean background value of GFP-positive particles in Gate 2 in mice infected with non-GFP expressing parasites (8.7%; 30 measurements) plus the standard deviation (2.7) multiplied by the critical value of a T-distribution (t_{cv} 2.01; P = 0.05; 29 degrees of freedom).

In addition, the proportion of Δ*smac* parasites relative to WT parasites was modeled using linear mixed effects models (Pinheiro and Bates). The proportion of Δ*smac* parasites was log-transformed to linearize the data. Thus, the fraction of Δ*smac* = $a + b \times t$, where a is the intercept, and b the proportion of Δ*smac* parasites per time unit (week, t). The antilog of this equation is: fraction Δ*smac* = $e^{a+b\times t}$, which can be written as $(e^a)\times(e^{b\times t})$ where the antilog of parameter b (e^b) represents the relative change in the proportion of Δ*smac* parasites per time unit. Data of this analysis are presented as the relative change in the proportion of Δ*smac* parasites per time unit (antilog of parameter b) with 95% confidence intervals (Table S6). Modeling was initiated using a simple model without random effects for the parameters and was subsequently refined in a stepwise manner by the addition of random effects for intercept or slope. Model fits were evaluated comparing Aikake Information Criterion (AIC) obtained by maximum likelihood estimation. (ML) models with the lowest AIC were selected as final models. Parameters for the best fitting models were then finalized using restricted maximum likelihood (REML).

For splenectomy, naive mice under painkiller (Temgesic, 0.15 mg/body weight) were anaesthetized using isoflurane and the spleen was removed. After a small lateral incision, the spleen was pulled out and splenic blood vessels were ligatured. The spleen was then removed by transecting the blood vessel distal to the ligature. The skin incision was closed using wound clips. Splenectomized mice were used in the GR assay 1 wk after the spleens were removed.

Statistical methods. Statistical analysis were performed using Student's *t* test with the Prism software package 5 (GraphPad Software) and Student's *t* test with R software (R foundation for Statistical Computing, Vienna, Austria).

Online supplemental material. Fig. S1 shows a schematic representation of constructs used for generation of transgenic *P. berghei ANKA* parasites and parasites lacking expression of SMAC (Δ*smac1* and Δ*smac2*). Fig. S2 shows the generation of the selectable marker free line Δ*smac3*$^{-sm}$ and *smac* complementation (Δ*smac3*+*smac*). Fig. S3 shows in vivo imaging of schizonts in mice infected with Δ*smac3*$^{-sm}$ and complemented Δ*smac3*+*smac* parasites in WT mice. Fig. S4 presents survival of the Δsmac parasites in mixed infections in GR assays in nonsplenectomized and splenectomized WT and KO mice. Table S1 presents HMM searches for *P. falciparum* and *P. berghei ANKA* proteins containing CIDR and DBL domains and for *P. berghei ANKA* proteins containing the PEXEL motif within the first 100 aa. Table S2 lists proteins identified by proteome analyses of proteins associated with the membranes of irbc containing the schizont stage. Table S3 lists the number of proteins in the HL and SS proteomes (Table S2) and in the complete *P. berghei ANKA* genome that show export features. Table S4 presents the characteristics of 30 proteins selected for functional analysis by targeted gene deletion and genotype and phenotype characteristics of 19 gene deletion mutants. Table S5 shows the sequence of primers used in this study. Table S6 displays estimates of the relative change of the ratio of Δ*smac* and WT parasites in mixed infections in the GR assays (Fig. 4 and Fig. S5) using linear mixed effects models. Online supplemental material is available at http://www.jem.org/cgi/content/full/jem.20110762/DC1.

We would like to thank Maaike van Dooren, Ivo Que, Elena Aime, Peter Neeskens, Frans Prins, Ramon Arens, and Michel Mulders for excellent technical support. We thank Dr. Maria Febbraio for permission to use the CD36$^{-/-}$ mice.

The work was supported by a grant from The Netherlands Organization for Scientific Research (ZonMW TOP grant number 9120_6135). J.A.M. Braks is supported by the European Community's Seventh Framework Program (FP7/2007-2013) under grant agreement no. 201222. C.H.M. Kocken and C.J Janse are supported by grants of the European Community's Seventh Framework Program (FP7/2007-2013) under grant agreement no. 242095.

The authors have no conflicting financial interests.

Submitted: 18 April 2011
Accepted: 22 November 2011

REFERENCES

Aikawa, M., A. Brown, C.D. Smith, T. Tegoshi, R.J. Howard, T.H. Hasler, Y. Ito, G. Perry, W.E. Collins, and K. Webster. 1992. A primate model for human cerebral malaria: *Plasmodium coatneyi*-infected rhesus monkeys. *Am. J. Trop. Med. Hyg.* 46:391–397.

Aitman, T.J., L.D. Cooper, P.J. Norsworthy, F.N. Wahid, J.K. Gray, B.R. Curtis, P.M. McKeigue, D. Kwiatkowski, B.M. Greenwood, R.W. Snow, et al. 2000. Malaria susceptibility and CD36 mutation. *Nature.* 405:1015–1016. http://dx.doi.org/10.1038/35016636

Avril, M., M.M. Cartwright, M.J. Hathaway, M. Hommel, S.R. Elliott, K. Williamson, D.L. Narum, P.E. Duffy, M. Fried, J.G. Beeson, and J.D. Smith. 2010. Immunization with VAR2CSA-DBL5 recombinant protein elicits broadly cross-reactive antibodies to placental *Plasmodium falciparum*-infected erythrocytes. *Infect. Immun.* 78:2248–2256. http://dx.doi.org/10.1128/IAI.00410-09

Barnwell, J.W., R.J. Howard, and L.H. Miller. 1982. Altered expression of *Plasmodium knowlesi* variant antigen on the erythrocyte membrane in splenectomized rhesus monkeys. *J. Immunol.* 128:224–226.

Barnwell, J.W., R.J. Howard, H.G. Coon, and L.H. Miller. 1983. Splenic requirement for antigenic variation and expression of the variant antigen on the erythrocyte membrane in cloned *Plasmodium knowlesi* malaria. *Infect. Immun.* 40:985–994.

Braks, J.A., B. Franke-Fayard, H. Kroeze, C.J. Janse, and A.P. Waters. 2006. Development and application of a positive-negative selectable marker system for use in reverse genetics in *Plasmodium*. *Nucleic Acids Res.* 34: e39. http://dx.doi.org/10.1093/nar/gnj033

Buffet, P.A., I. Safeukui, G. Deplaine, V. Brousse, V. Prendki, M. Thellier, G.D. Turner, and O. Mercereau-Puijalon. 2011. The pathogenesis of *Plasmodium falciparum* malaria in humans: insights from splenic physiology. *Blood.* 117:381–392. http://dx.doi.org/10.1182/blood-2010-04-202911

Bull, P.C., A. Pain, F.M. Ndungu, S.M. Kinyanjui, D.J. Roberts, C.I. Newbold, and K. Marsh. 2005. *Plasmodium falciparum* antigenic variation:

relationships between in vivo selection, acquired antibody response, and disease severity. *J. Infect. Dis.* 192:1119–1126. http://dx.doi.org/10.1086/432761

Chakravorty, S.J., and A. Craig. 2005. The role of ICAM-1 in *Plasmodium falciparum* cytoadherence. *Eur. J. Cell Biol.* 84:15–27. http://dx.doi.org/10.1016/j.ejcb.2004.09.002

Dondorp, A.M., P.A. Kager, J. Vreeken, and N.J. White. 2000. Abnormal blood flow and red blood cell deformability in severe malaria. *Parasitol. Today* (*Regul. Ed.*). 16:228–232. http://dx.doi.org/10.1016/S0169-4758(00)01666-5

Dufresne, A.T., and M. Gromeier. 2004. A nonpolio enterovirus with respiratory tropism causes poliomyelitis in intercellular adhesion molecule 1 transgenic mice. *Proc. Natl. Acad. Sci. USA.* 101:13636–13641. http://dx.doi.org/10.1073/pnas.0403998101

Engwerda, C.R., L. Beattie, and F.H. Amante. 2005. The importance of the spleen in malaria. *Trends Parasitol.* 21:75–80. http://dx.doi.org/10.1016/j.pt.2004.11.008

Franke-Fayard, B., C.J. Janse, M. Cunha-Rodrigues, J. Ramesar, P. Büscher, I. Que, C. Löwik, P.J. Voshol, M.A. den Boer, S.G. van Duinen, et al. 2005. Murine malaria parasite sequestration: CD36 is the major receptor, but cerebral pathology is unlinked to sequestration. *Proc. Natl. Acad. Sci. USA.* 102:11468–11473. http://dx.doi.org/10.1073/pnas.0503386102

Franke-Fayard, B., A.P. Waters, and C.J. Janse. 2006. Real-time in vivo imaging of transgenic bioluminescent blood stages of rodent malaria parasites in mice. *Nat. Protoc.* 1:476–485. http://dx.doi.org/10.1038/nprot.2006.69

Franke-Fayard, B., J. Fonager, A. Braks, S.M. Khan, and C.J. Janse. 2010. Sequestration and tissue accumulation of human malaria parasites: can we learn anything from rodent models of malaria? *PLoS Pathog.* 6:e1001032. http://dx.doi.org/10.1371/journal.ppat.1001032

Fried, M., and P.E. Duffy. 1996. Adherence of *Plasmodium falciparum* to chondroitin sulfate A in the human placenta. *Science.* 272:1502–1504. http://dx.doi.org/10.1126/science.272.5267.1502

Goldberg, D.E., and A.F. Cowman. 2010. Moving in and renovating: exporting proteins from *Plasmodium* into host erythrocytes. *Nat. Rev. Microbiol.* 8:617–621. http://dx.doi.org/10.1038/nrmicro2420

Graewe, S., S. Retzlaff, N. Struck, C.J. Janse, and V.T. Heussler. 2009. Going live: a comparative analysis of the suitability of the RFP derivatives RedStar, mCherry and tdTomato for intravital and in vitro live imaging of *Plasmodium* parasites. *Biotechnol. J.* 4:895–902. http://dx.doi.org/10.1002/biot.200900035

Hall, N., M. Karras, J.D. Raine, J.M. Carlton, T.W. Kooij, M. Berriman, L. Florens, C.S. Janssen, A. Pain, G.K. Christophides, et al. 2005. A comprehensive survey of the *Plasmodium* life cycle by genomic, transcriptomic, and proteomic analyses. *Science.* 307:82–86. http://dx.doi.org/10.1126/science.1103717

Hirosawa, M., M. Hoshida, M. Ishikawa, and T. Toya. 1993. MASCOT: multiple alignment system for protein sequences based on three-way dynamic programming. *Comput. Appl. Biosci.* 9:161–167.

Hiss, J.A., J.M. Przyborski, F. Schwarte, K. Lingelbach, and G. Schneider. 2008. The *Plasmodium* export element revisited. *PLoS ONE.* 3:e1560. http://dx.doi.org/10.1371/journal.pone.0001560

Janse, C.J., and A.P. Waters. 1995. *Plasmodium berghei*: the application of cultivation and purification techniques to molecular studies of malaria parasites. *Parasitol. Today* (*Regul. Ed.*). 11:138–143. http://dx.doi.org/10.1016/0169-4758(95)80133-2

Janse, C.J., A. Haghparast, M.A. Sperança, J. Ramesar, H. Kroeze, H.A. del Portillo, and A.P. Waters. 2003. Malaria parasites lacking eef1a have a normal S/M phase yet grow more slowly due to a longer G1 phase. *Mol. Microbiol.* 50:1539–1551. http://dx.doi.org/10.1046/j.1365-2958.2003.03820.x

Janse, C.J., J. Ramesar, and A.P. Waters. 2006. High-efficiency transfection and drug selection of genetically transformed blood stages of the rodent malaria parasite *Plasmodium berghei*. *Nat. Protoc.* 1:346–356. http://dx.doi.org/10.1038/nprot.2006.53

John, C.C., E. Kutamba, K. Mugarura, and R.O. Opoka. 2010. Adjunctive therapy for cerebral malaria and other severe forms of *Plasmodium falciparum* malaria. *Expert Rev. Anti Infect. Ther.* 8:997–1008. http://dx.doi.org/10.1586/eri.10.90

Kersey, P.J., J. Duarte, A. Williams, Y. Karavidopoulou, E. Birney, and R. Apweiler. 2004. The International Protein Index: an integrated database for proteomics experiments. *Proteomics.* 4:1985–1988. http://dx.doi.org/10.1002/pmic.200300721

Khan, S.M., B. Franke-Fayard, G.R. Mair, E. Lasonder, C.J. Janse, M. Mann, and A.P. Waters. 2005. Proteome analysis of separated male and female gametocytes reveals novel sex-specific *Plasmodium* biology. *Cell.* 121:675–687. http://dx.doi.org/10.1016/j.cell.2005.03.027

Krücken, J., L.I. Mehnert, M.A. Dkhil, M. El-Khadragy, W.P. Benten, H. Mossmann, and F. Wunderlich. 2005. Massive destruction of malaria-parasitized red blood cells despite spleen closure. *Infect. Immun.* 73:6390–6398. http://dx.doi.org/10.1128/IAI.73.10.6390-6398.2005

Langhorne, J., F.R. Albano, M. Hensmann, L. Sanni, E. Cadman, C. Voisine, and A.M. Sponaas. 2004. Dendritic cells, pro-inflammatory responses, and antigen presentation in a rodent malaria infection. *Immunol. Rev.* 201:35–47. http://dx.doi.org/10.1111/j.0105-2896.2004.00182.x

Maier, A.G., B.M. Cooke, A.F. Cowman, and L. Tilley. 2009. Malaria parasite proteins that remodel the host erythrocyte. *Nat. Rev. Microbiol.* 7:341–354. http://dx.doi.org/10.1038/nrmicro2110

Marti, M., R.T. Good, M. Rug, E. Knuepfer, and A.F. Cowman. 2004. Targeting malaria virulence and remodeling proteins to the host erythrocyte. *Science.* 306:1930–1933. http://dx.doi.org/10.1126/science.1102452

Mebius, R.E., and G. Kraal. 2005. Structure and function of the spleen. *Nat. Rev. Immunol.* 5:606–616. http://dx.doi.org/10.1038/nri1669

Miller, L.H., M.F. Good, and G. Milon. 1994. Malaria pathogenesis. *Science.* 264:1878–1883. http://dx.doi.org/10.1126/science.8009217

Miller, L.H., D.I. Baruch, K. Marsh, and O.K. Doumbo. 2002. The pathogenic basis of malaria. *Nature.* 415:673–679. http://dx.doi.org/10.1038/415673a

Mishra, S.K., and C.R. Newton. 2009. Diagnosis and management of the neurological complications of *falciparum* malaria. *Nat Rev Neurol.* 5:189–198. http://dx.doi.org/10.1038/nrneurol.2009.23

Moore, B.R., J.D. Jago, and K.T. Batty. 2008. *Plasmodium berghei*: parasite clearance after treatment with dihydroartemisinin in an asplenic murine malaria model. *Exp. Parasitol.* 118:458–467.

Mota, M.M., W. Jarra, E. Hirst, P.K. Patnaik, and A.A. Holder. 2000. *Plasmodium chabaudi*-infected erythrocytes adhere to CD36 and bind to microvascular endothelial cells in an organ-specific way. *Infect. Immun.* 68:4135–4144. http://dx.doi.org/10.1128/IAI.68.7.4135-4144.2000

Olsen, J.V., and M. Mann. 2004. Improved peptide identification in proteomics by two consecutive stages of mass spectrometric fragmentation. *Proc. Natl. Acad. Sci. USA.* 101:13417–13422. http://dx.doi.org/10.1073/pnas.0405549101

Pain, A., U. Böhme, A.E. Berry, K. Mungall, R.D. Finn, A.P. Jackson, T. Mourier, J. Mistry, E.M. Pasini, M.A. Aslett, et al. 2008. The genome of the simian and human malaria parasite *Plasmodium knowlesi*. *Nature.* 455:799–803. http://dx.doi.org/10.1038/nature07306

Pasini, E.M., M. Kirkegaard, P. Mortensen, H.U. Lutz, A.W. Thomas, and M. Mann. 2006. In-depth analysis of the membrane and cytosolic proteome of red blood cells. *Blood.* 108:791–801. http://dx.doi.org/10.1182/blood-2005-11-007799

Patel, S.N., L. Serghides, T.G. Smith, M. Febbraio, R.L. Silverstein, T.W. Kurtz, M. Pravenec, and K.C. Kain. 2004. CD36 mediates the phagocytosis of *Plasmodium falciparum*-infected erythrocytes by rodent macrophages. *J. Infect. Dis.* 189:204–213. http://dx.doi.org/10.1086/380764

Quinn, T.C., and D.J. Wyler. 1979. Intravascular clearance of parasitized erythrocytes in rodent malaria. *J. Clin. Invest.* 63:1187–1194. http://dx.doi.org/10.1172/JCI109413

Rappsilber, J., Y. Ishihama, and M. Mann. 2003. Stop and go extraction tips for matrix-assisted laser desorption/ionization, nanoelectrospray, and LC/MS sample pretreatment in proteomics. *Anal. Chem.* 75:663–670. http://dx.doi.org/10.1021/ac026117i

Rogerson, S.J., R. Tembenu, C. Dobaño, S. Plitt, T.E. Taylor, and M.E. Molyneux. 1999. Cytoadherence characteristics of *Plasmodium falciparum*-infected erythrocytes from Malawian children with severe and uncomplicated malaria. *Am. J. Trop. Med. Hyg.* 61:467–472.

Rogerson, S.J., L. Hviid, P.E. Duffy, R.F. Leke, and D.W. Taylor. 2007. Malaria in pregnancy: pathogenesis and immunity. *Lancet Infect. Dis.* 7:105–117. http://dx.doi.org/10.1016/S1473-3099(07)70022-1

Rowe, J.A., A. Claessens, R.A. Corrigan, and M. Arman. 2009. Adhesion of *Plasmodium falciparum*-infected erythrocytes to human cells: molecular mechanisms and therapeutic implications. *Expert Rev. Mol. Med.* 11:e16. http://dx.doi.org/10.1017/S1462399409001082

Sargeant, T.J., M. Marti, E. Caler, J.M. Carlton, K. Simpson, T.P. Speed, and A.F. Cowman. 2006. Lineage-specific expansion of proteins exported to erythrocytes in malaria parasites. *Genome Biol.* 7:R12. http://dx.doi.org/10.1186/gb-2006-7-2-r12

Sayles, P.C., A.J. Cooley, and D.L. Wassom. 1991. A spleen is not necessary to resolve infections with *Plasmodium yoelii*. *Am. J. Trop. Med. Hyg.* 44:42–48.

Scherf, A., J.J. Lopez-Rubio, and L. Riviere. 2008. Antigenic variation in *Plasmodium falciparum*. *Annu. Rev. Microbiol.* 62:445–470. http://dx.doi.org/10.1146/annurev.micro.61.080706.093134

Schofield, L., and G.E. Grau. 2005. Immunological processes in malaria pathogenesis. *Nat. Rev. Immunol.* 5:722–735. http://dx.doi.org/10.1038/nri1686

Serghides, L., and K.C. Kain. 2001. Peroxisome proliferator-activated receptor gamma-retinoid X receptor agonists increase CD36-dependent phagocytosis of *Plasmodium falciparum*-parasitized erythrocytes and decrease malaria-induced TNF-alpha secretion by monocytes/macrophages. *J. Immunol.* 166:6742–6748.

Sherman, I.W., S. Eda, and E. Winograd. 2003. Cytoadherence and sequestration in *Plasmodium falciparum*: defining the ties that bind. *Microbes Infect.* 5:897–909. http://dx.doi.org/10.1016/S1286-4579(03)00162-X

Silverstein, R.L., and M. Febbraio. 2009. CD36, a scavenger receptor involved in immunity, metabolism, angiogenesis, and behavior. *Sci. Signal.* 2:re3. http://dx.doi.org/10.1126/scisignal.272re3

Smith, J.D., G. Subramanian, B. Gamain, D.I. Baruch, and L.H. Miller. 2000. Classification of adhesive domains in the *Plasmodium falciparum* erythrocyte membrane protein 1 family. *Mol. Biochem. Parasitol.* 110:293–310. http://dx.doi.org/10.1016/S0166-6851(00)00279-6

Spaccapelo, R., C.J. Janse, S. Caterbi, B. Franke-Fayard, J.A. Bonilla, L.M. Syphard, M. Di Cristina, T. Dottorini, A. Savarino, A. Cassone, et al. 2010. Plasmepsin 4-deficient *Plasmodium berghei* are virulence attenuated and induce protective immunity against experimental malaria. *Am. J. Pathol.* 176:205–217. http://dx.doi.org/10.2353/ajpath.2010.090504

Srivastava, A., S. Gangnard, A. Round, S. Dechavanne, A. Juillerat, B. Raynal, G. Faure, B. Baron, S. Ramboarina, S.K. Singh, et al. 2010. Full-length extracellular region of the var2CSA variant of PfEMP1 is required for specific, high-affinity binding to CSA. *Proc. Natl. Acad. Sci. USA.* 107:4884–4889. http://dx.doi.org/10.1073/pnas.1000951107

Tanke, H.J., J. Wiegant, R.P. van Gijlswijk, V. Bezrookove, H. Pattenier, R.J. Heetebrij, E.G. Talman, A.K. Raap, and J. Vrolijk. 1999. New strategy for multi-colour fluorescence in situ hybridisation: COBRA: COmbined Binary RAtio labelling. *Eur. J. Hum. Genet.* 7:2–11. http://dx.doi.org/10.1038/sj.ejhg.5200265

Terrazas, C.A., L.I. Terrazas, and L. Gómez-García. 2010. Modulation of dendritic cell responses by parasites: a common strategy to survive. *J. Biomed. Biotechnol.* 2010:357106.

Urban, B.C., D.J. Ferguson, A. Pain, N. Willcox, M. Plebanski, J.M. Austyn, and D.J. Roberts. 1999. *Plasmodium falciparum*-infected erythrocytes modulate the maturation of dendritic cells. *Nature.* 400:73–77. http://dx.doi.org/10.1038/21900

Wilm, M., A. Shevchenko, T. Houthaeve, S. Breit, L. Schweigerer, T. Fotsis, and M. Mann. 1996. Femtomole sequencing of proteins from polyacrylamide gels by nano-electrospray mass spectrometry. *Nature.* 379:466–469. http://dx.doi.org/10.1038/379466a0